Composites Communications 48 (2024) 101919

Contents lists available at ScienceDirect

Composites Communications

journal homepage: www.elsevier.com/locate/coco

Short Communication

# Natural biopolymer/$CuInS_2$ quantum dot-based red emissive, physically transient, and dynamically self-polarized piezoelectrets

Zhu Liu [a,b], Yu Lai [a,b], Juan Li [b], Zhipei Xia [b], Liang Lu [a,b], Chuanfeng Wang [a,b], Biyao Huang [b], Chu Pan [b], Jiashun Wen [b], Weiqing Yang [a,c,**], Jun Lu [a,b,*,1]

[a] Key Laboratory of Advanced Technologies of Materials, Ministry of Education, School of Materials Science and Engineering, Southwest Jiaotong University, Chengdu, 610031, Sichuan, China
[b] School of Chemistry, Southwest Jiaotong University, Chengdu, 610031, Sichuan, China
[c] Research Institute of Frontier Science, Southwest Jiaotong University, Chengdu, 610031, Sichuan, China

ARTICLE INFO

*Keywords:*
Multifunction integrated composites
Polyhydroxybutyrate
Cellulose nanocrystals
$CuInS_2$ quantum dots
Electrospinning
Electrical properties

ABSTRACT

Here, we report a novel class of electret-transducer materials developed by electrospinning copper indium disulfide ($CuInS_2$) quantum dots (CIS-QDs), sulfonated cellulose nanocrystals (S–CNCs), and microbial polyhydroxybutyrate (PHB). The piezoelectret materials consist of CIS-QDs/S–CNCs/PHB-based highly-oriented electret fibers. The striking merits include large Stokes shifted red-luminescence, composting environment degradation, and dynamic self-polarization-enhanced piezoresponse. The first use of $CuInS_2$-based QDs for doping in natural biopolymers suggests that the CIS-QDs allow for preferential orientation growth of piezoelectric phase PHB lamellae in bio-based electret fibers. The synergistic action of CIS-QDs-constrained, highly-oriented PHB micro-dipoles and dynamically-active S–CNCs macro-dipoles further enables a significantly enhanced piezoelectric response of the piezoelectrets. The piezoelectric output of red-emission CIS-QDs/S–CNCs/PHB-based nanogenerator is almost 2 and 5 times higher than that of S–CNCs/PHB-based and PHB-based devices, respectively. Moreover, the flexible self-powered device possesses the ability to collect and analyze athletic big data in intelligent sports. This class of versatile, ecologically decomposable piezoelectrets could be compelling building materials for applications in digital-twin- and metaverse-based ecosystems.

## 1. Introduction

The rapid evolving of artificial intelligence (AI), and the increasing integration of AI with functional electronics have given birth to a new breed of intelligent systems in the era of the 5G/internet of things (IoTs) [1–5]. Examples include digital-twin- and metaverse-based ecosystems [1–5]. Digital twins, one of the basic building blocks of metaverse, are digital equivalents in cyber space to physical objects in real space [1–5]. They have broad application prospects in the realization of smart homes, smart industry, smart cities, and so on [1–5]. To construct a digital-twin-based system requires a huge number of electronic sensors with diversified functions distributed in physical scenarios to achieve seamless data transmission [1–5]. Using conventional devices will inevitably face two thorny problems: extremely high power consumption and e-waste disposal. Therefore, the self-powered, physically transient, and multifunctional devices are one of the feasible solutions to realize the self-sustainable, low-power digital twin systems [1–9]. These devices are made from decomposable, multifunctional energy materials with a specific life cycle. After use, all or part of a device can physically disappear at a controlled rate by means of environmental degradation or solvent dissolution [6–9]. Nevertheless, there is so far a very limited number of available transient energy materials with multiple functionalities.

Naturally occurring piezoelectric biopolymers, for example, cellulose [10–14], and polyhydroxyalkanoates (PHAs) [10,15–17], possess unique features that make them promising constituent materials for self-powered, eco-friendly transient devices. They are naturally abundant, environmentally sustainable, and highly biocompatible/biodegradable [10–17]. In particular, under benign conditions, the microorganism-produced PHAs can be processed into

* Corresponding author.
** Corresponding author.
*E-mail addresses:* wqyang@swjtu.edu.cn (W. Yang), junluprc@hotmail.com (J. Lu).
[1] Other used names Jun Lv and Jun Lyu.

https://doi.org/10.1016/j.coco.2024.101919
Received 28 March 2024; Received in revised form 26 April 2024; Accepted 26 April 2024
Available online 27 April 2024

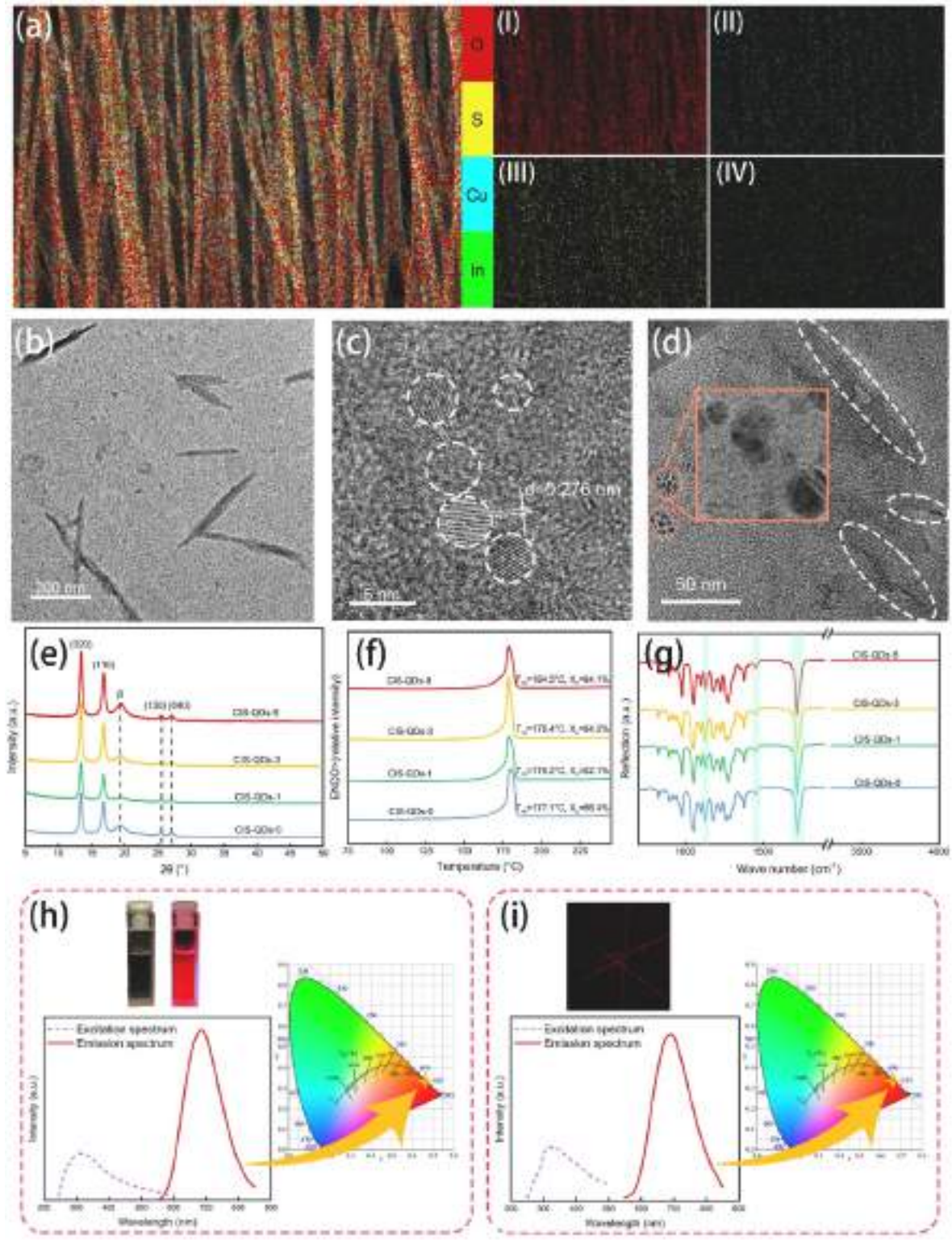


**Fig. 1.** (a) Representative EDS mapping images of CIS-QDs/S–CNCs/PHB fibers showing O (red), Cu (blue),S (yellow) and In (green) distributions. (b) TEM of S–CNCs in water. (c) TEM of CIS-QDs in chloroform. The lattice spacing of 0.276 nm corresponds to the $CuInS_2$ (200) plane. (d) Typical TEM showing the dispersion and morphology of S–CNCs and CIS-QDs in CIS-QDs/S–CNCs/PHB fibers. (e) XRD, (f) DSC, and (g) FTIR of CIS-QDs-x fibers. (h) PL excitation/emission spectra and CIE diagram of CIS-QDs. The top inset shows the digital pictures of pristine chloroform (left) and CIS-QDs/chloroform solution (right) under ultraviolet light ($\lambda_{ex}$: 365 nm). (i) PL excitation/emission spectra and CIE diagram of CIS-QDs/S–CNCs/PHB. The top inset shows the laser scanning confocal microscopy image of electrospun CIS-QDs/S–CNCs/PHB fibers ($\lambda_{ex}$: 400 nm). (For interpretation of the references to color in this figure legend, the reader is referred to the Web version of this article.)

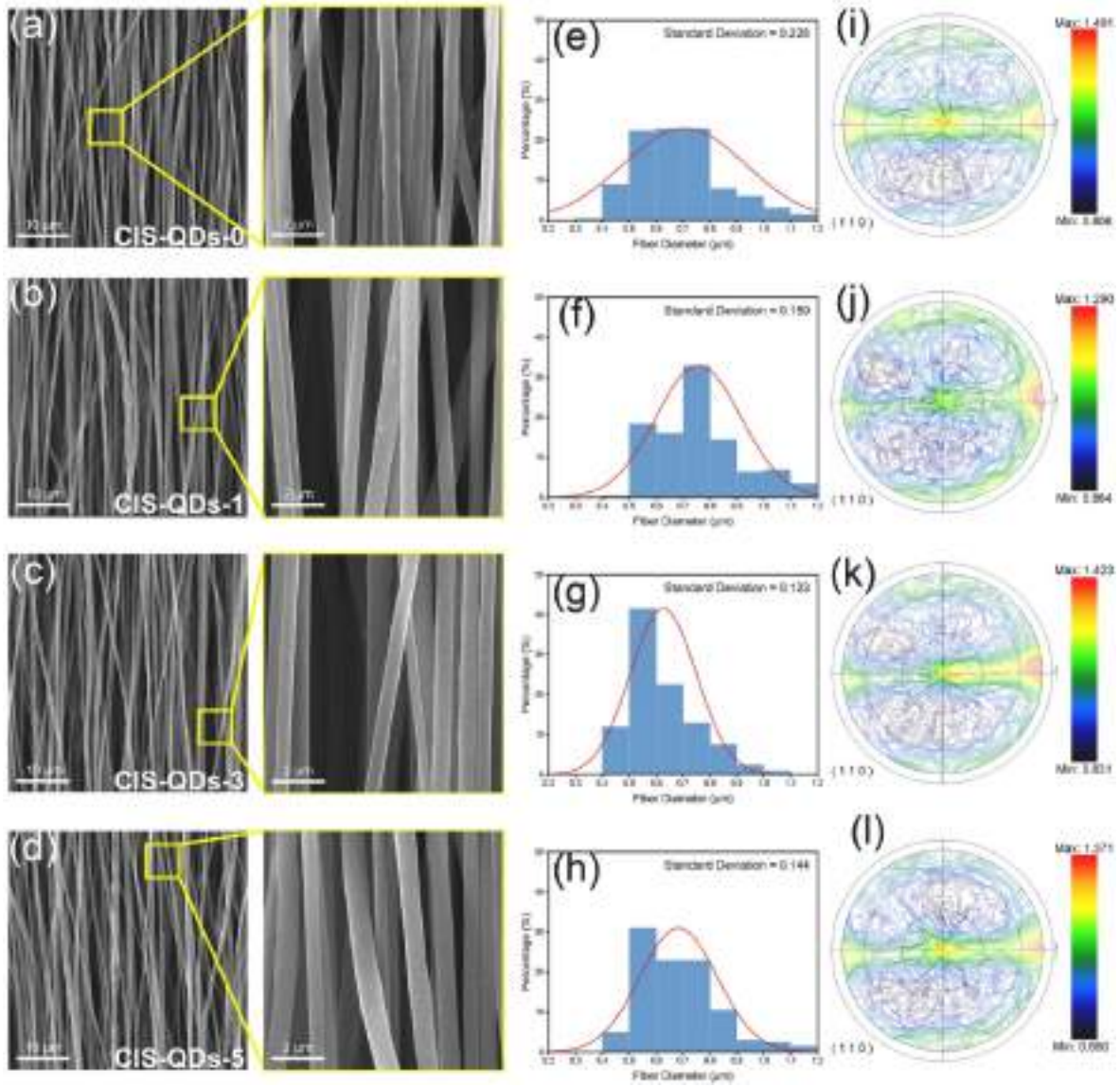


**Fig. 2.** SEM of (a) CIS-QDs-0, (b) CIS-QDs-1, (c) CIS-QDs-3, and (d) CIS-QDs-5 fibers. Diameter distribution of (e) CIS-QDs-0, (f) CIS-QDs-1, (g) CIS-QDs-3, and (h) CIS-QDs-5 fibers. X-ray pole figures of PHB (110) crystal plane in (i) CIS-QDs-0, (j) CIS-QDs-1, (k) CIS-QDs-3, and (l) CIS-QDs-5 fibers. Note the vertical color bars show the intensities of XRD pole figures. (For interpretation of the references to color in this figure legend, the reader is referred to the Web version of this article.)

various forms of device components with tunable materials properties [11,15–17]. Unfortunately, the very weak piezoelectric response of PHAs remains an obstacle to large-scale device applications [8,9,17]. The origin of piezoelectricity of PHAs is the chiral carbon-associated molecular dipole in the asymmetry crystalline structure [9,17]. Usually, a higher degree of crystalline ordering is correlated with a higher level of piezoelectric output [9,17]. In this regard, the piezoelectric enhancement as well as functional enrichment can be achieved by the design/processing of a novel class of PHAs-based biocomposites.

Copper indium disulfide ($CuInS_2$) quantum dots (CIS-QDs) are emerging eco-friendly I-III-VI semiconductor QDs [18–20]. The attractive merits include tunable photoluminescence (PL) emission, ranging from visible to near infrared (NIR) regions, a large Stokes shift, and non-toxic elements [18–20]. Sulfonated cellulose nanocrystals (S–CNCs) are one of the anionic polysaccharide derivatives produced by sulfuric acid hydrolysis of natural plant cellulose [17]. They can serve as a charged biological nanofiller to improve the electrical output of bio-based materials [17,21]. Here, we develop a red luminescent, physically transient, and dynamically self-polarized piezoelectret by electrospinning $CuInS_2$ quantum dots, S–CNCs, and polyhydroxybutyrate (PHB), a mass-produced microbial PHA member (Fig. S1a). This new class of multifunctional electret-transducer materials are in the form of free-standing thin films consisting of highly oriented, electrospun CIS-QDs/S–CNCs/PHB-based electret fibers. The piezoelectret films are integrated into a prototype piezoelectret nanogenerator to evaluate the piezoelectric characteristics (Figs. S1b–d). The proof-of-concept device demonstrates a significantly enhanced piezoelectric response as an energy harvester and a self-powered sensor in specific scenarios.

## 2. Experimental

The detailed experimental process is presented in the Supporting Information.

## 3. Results and discussion

In the CIS-QDs/S–CNCs/PHB-based electret fibers, the successful incorporation and an overall good dispersion of both CIS-QDs and S–CNCs were confirmed using energy dispersive spectroscopy (EDS)

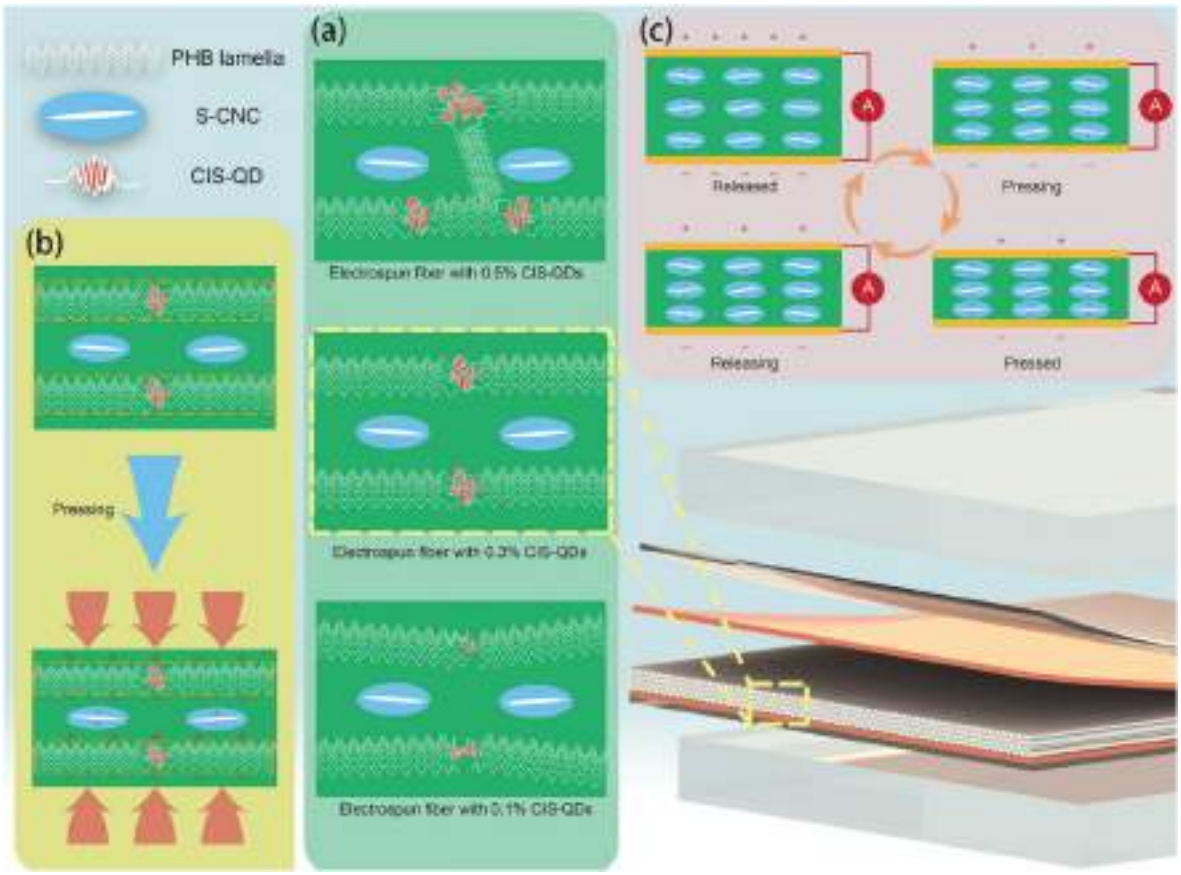


**Fig. 3.** (a) Schematic diagram illustrating the effect of CIS-QDs content on the orientation of PHB piezo-phase crystalline lamellae in the electrospun CIS-QDs-x fibers. (b) Schematic illustration of the composite structure and the working mechanism of the CIS-QDs/S–CNCs/PHB-based dynamically self-polarized piezoelectret. (c) Schematic drawing of the operation mechanism of the dynamic piezoelectret nanogenerator based on CIS-QDs/S–CNCs/PHB nanofibers.

(Fig. 1a and S2) and transmission electron microscopy (TEM) (Fig. 1b–d and S3). The clear lattice fringes revealed by high-resolution TEM indicate the high crystallinity of CIS-QDs (Fig. 1c and S3). Also, the CIS-QDs are prone to self-organize in the PHB matrix to form hierarchical nanoscale assemblies (Fig. 1d and S3). To our knowledge, this is the first doping using $CuInS_2$-based QDs in natural biopolymers. Hence, the effect of CIS-QDs concentration was further investigated using X-rays diffraction (XRD), differential scanning calorimetry (DSC), and Fourier transform infrared (FTIR) spectrometer, respectively (Fig. 1e–g). The CIS-QDs/S–CNCs/PHB-based fibers with various CIS-QDs contents are denoted here as CIS-QDs-x. The x represents the mass fraction of CIS-QDs to PHB, namely x CIS-QDs per thousand PHB. The XRD diffractograms provide the evidence the crystal form of PHB remains unchanged in the presence of CIS-QDs (Fig. 1e). The DSC data verify the highly crystalline nature of the electret fibers (Fig. 1f). Moreover, the IR spectra indicate in the electret fibers the CIS-QDs, S–CNCs, and PHB are actually combined by physical rather than chemical interactions (Fig. 1g).

Fig. 1h shows the PL excitation/emission spectra and chromaticity coordinates of CIS-QDs. The coordinates were calculated using the 1931 CIE (International Commission on Illumination) system. The CIS-QDs emit high-purity red light with the optimal excitation wavelength at 310 nm and the optimal emission wavelength at 690 nm, respectively. The PL quantum yield (QY) was determined to be 31.96 % (Fig. S4a). Fig. 1i shows the PL excitation/emission spectra and CIE diagram of CIS-QDs/S–CNCs/PHB. Interestingly, with excitation/emission peaks at 315/690 nm, the red emissive CIS-QDs/S–CNCs/PHB possessed a considerably high PL QY of 52.33 % (Fig. S4b). The enhanced PL QY may be attributed to the interactions between CIS-QDs, S–CNCs and PHB molecules. The fluorescence image in Fig. 1i further confirms the red-emission electret fibers were manufactured successfully.

The diameter, morphology, and orientation of electrospun fibers are directly related to the performance of the fibers and fiber-based devices in practical applications [22–25]. Many studies have confirmed that uniform morphology, narrow diameter distribution and preferred orientation are beneficial to improving the piezoelectric strength of these piezoelectric materials-based electrospun fibers [17,24,25]. Fig. 2 shows the scanning electron microscopy (SEM) images, diameter distribution, and X-ray pole figures of the electrospun CIS-QDs-x-based electret fibers. As a reference, the pristine PHB-based electrospun fibers were prepared and characterized in the same way as for the CIS-QDs-x fibers (Fig. S5). Evidently, the electret fibers are bead-free, smooth, and they are highly uniaxially oriented (Fig. 2a–d). Among these samples, the CIS-QDs-3 fibers have a smaller fiber diameter and a relatively narrow distribution in the diameter (Fig. 2e–h). Also, the measured X-ray pole figures of PHB (110) crystal plane, which is a direct visualization of the crystal orientation [26,27], confirm the very strong texture of the electret fibers (Fig. 2i-l). Especially, with a relatively small polar density region, the CIS-QDs-3 fiber has the highest maximum pole density in all the samples. This indicates the highest level of preferred crystal orientation of internal piezo-phase PHB lamellae [17,26]. Moreover, the CIS-QDs-3-based fiber film demonstrates the optimal mechanical performance in these CIS-QDs-x-based fiber films (Fig. S6). The CIS-QDs-3-based film was further placed in a well-fermented compost material. Notably, the self-standing fiber film was fully degraded in the composting material, and it disappeared from the composting degradation within 4 days (Fig. S7). Thus, these uniform, highly double-oriented electret fibers are a very valuable transient material for constructing highly piezo-responsive transient devices.

Fig. 3a shows a schematic diagram depicting the orientation growth of piezo-phase PHB lamellae under the constraints of different numbers

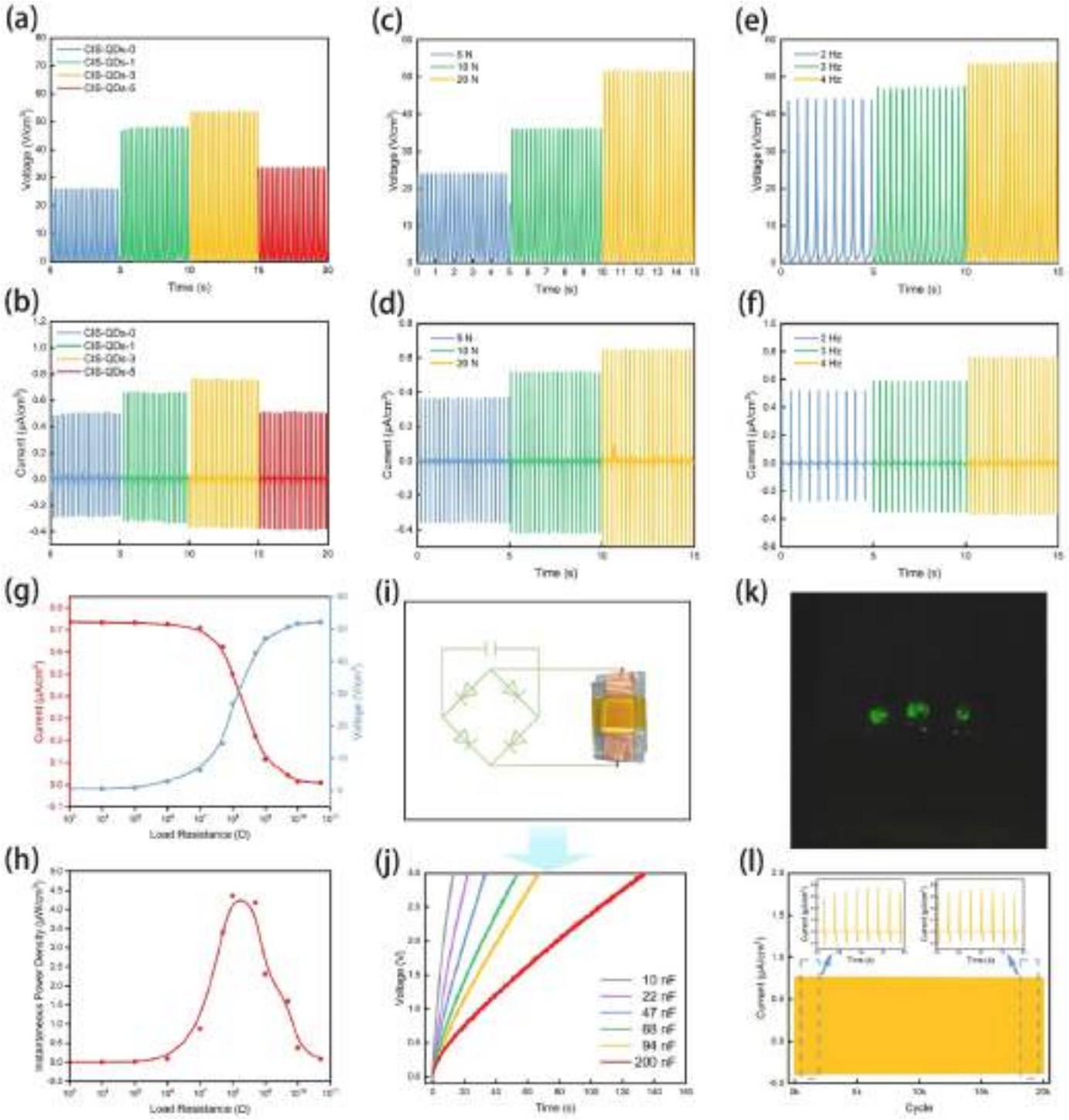


**Fig. 4.** Measured characteristics of piezoelectric output of CIS-QDs-x fiber based dynamic piezoelectret nanogenerator. The device area is 15 mm × 15 mm, and the piezoactive layer thickness is 0.375 mm. (a) Open-circuit voltage and (b) short-circuit current of CIS-QDs-x devices, with different CIS-QDs contents, stimulated using a 20-N and 4-Hz impulse force. (c) Open-circuit voltage and (d) short-circuit current of CIS-QDs-3 device, stimulated at different impulse forces and a fixed frequency of 4.0 Hz. (e) Open-circuit voltage and (f) short-circuit current of CIS-QDs-3 device, stimulated at different frequencies and a fixed impulse force of 20 N. (g) output voltage and output current, and (h) calculated power density of CIS-QDs-3 device at different external loads. (i) Equivalent circuit for charging a capacitor. (j) Charging curves of different commercial capacitors using CIS-QDs-3 device. (k) Digital picture showing the instant glow of green LEDs, using the power generated by the CIS-QDs-3 device under finger tapping. (l) Cyclic stability test of CIS-QDs-3 device for 20 000 cycles, whole signal, under the stimulation of a 20-N and 4-Hz impulse force. (For interpretation of the references to color in this figure legend, the reader is referred to the Web version of this article.)

of $CuInS_2$-based QDs. An excessively small number of CIS-QDs allows partially oriented growth, while an excessive inclusion of CIS-QDs leads to misorientation growth. In contrast, using moderate amounts of CIS-QDs achieves the highly-preferred orientation growth. A self-polarized piezoelectret nanogenerator was fabricated using the CIS-QDs-x fiber films as a piezoelectret material. Fig. 3b and c shows the working mechanism of this class of piezoelectrets and piezoelectret nanogenerators, respectively. Distinct from the voided charged polymer-

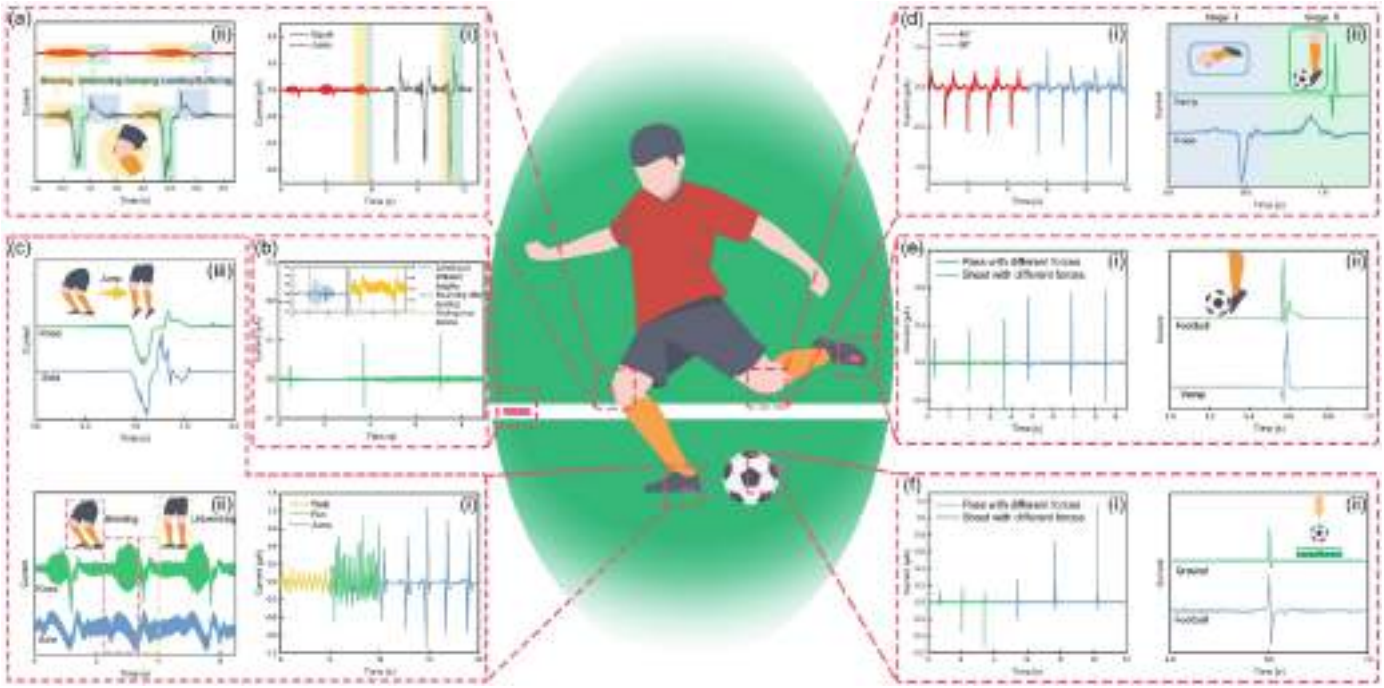

**Fig. 5.** In the actual scene of football practice, demonstration of CIS-QDs-3-based device as a flexible self-powered piezo-sensor for intelligent sports applications. By attaching the device to athlete's body, football and football ground, respectively, it is capable of precisely sensing the football practice activities in real time. (a) Piezo-signals generated by the device on athlete's knee while squatting and jumping: (a–i) real-time output of characteristic piezo-signals and (a-ii) comparison analysis of the two piezo-signals. (b) Piezo-signals produced by the device on football ground when football falls, bounces and rolls. (c) Comparison of piezo-signals by the device on (c–i) athlete's sole while walking, running and jumping, and by the device on athlete's sole and athlete's knee while (c-ii) squatting and (c-iii) jumping. (d) Comparison of piezo-signals by the device on (d–i) athlete's knee during bending at different angles, and by the device on (d-ii) athlete's knee and athlete's instep during shooting action. (e) Comparison of piezo-signals by the device on (e–i) athlete's instep during passing and shooting, and by the device on (e-ii) athlete's instep and football during shooting. (f) Comparison of output piezo-signals by the device on (f–i) football during passing and shooting, and by the device on (f-ii) football and football ground upon ball landing.

based piezoelectrets [28], the CIS-QDs-x-based piezoelectrets were directly used without any ultrahigh-voltage poling treatment. Under dynamic mechanical stimuli, the piezoelectric potential, generated by the deformation and relaxation of CIS-QDs-constrained, highly-oriented piezoelectric PHB crystals, enables the dissociation/separation of hydrogen cations/sulfonic anions in the sulphonic acid groups of S–CNCs (Fig. 3b). Then the S–CNCs can act as an artificial, dynamically-active macro-dipole. They play the same role as the charged voids of these foamed piezoelectrets [17,21,28]. The durable/stable mechanical-to-electrical conversion of a red-emissive piezoelectret nanogenerator thus can be achieved by the synergistic action of CIS-QDs-constrained intrinsic PHB molecular micro-dipoles and artificial S–CNCs macro-dipoles (Fig. 3c).

The piezoelectric characteristics of CIS-QDs-x-based nanogenerators were evaluated by measuring electrical output under impulse forces. The piezoelectric output of different devices is proportional to the level of the PHB crystal orientation constrained by $CuInS_2$-based QDs (Fig. 4a and b). Under a 20-N, 4-Hz impulse force, the output voltage and output current of CIS-QDs-3-based device reach 53 V $cm^{-3}$ and 0.76 μA $cm^{-3}$, respectively. The piezoelectric output is almost 2 and 5 times higher than that of the S–CNCs/PHB-based device and the pristine PHB-based device, respectively (Fig. S8). The device also shows stress- and frequency-dependent piezoelectric responses (Fig. 4c–f). The piezoelectric output increases with an increase of amplitude/frequency of impulse forces. The measured piezoelectric power density reaches a maximum of 4.5 μW $cm^{-3}$ at an external load resistance of 100 MΩ (Fig. 4g and h). Using the generated power, the device is able to quickly charge commercial capacitors (Fig. 4i and j), and directly operate commercial light-emitting diodes (LEDs) (Fig. 4k). Moreover, the device shows a highly durable, highly reproducible piezoelectric output in over 20 000 cycles (Fig. 4l).

The CIS-QDs-3-based piezoelectric device is mechanically flexible, and shape adaptable. It can distinguish between small pressure differences in human muscle actions. This allows the precise sensing of subtle human physiology, such as human joint motions, human facial expressions, and human throat movements (Fig. S9). As a proof of concept, in the real scene of football practice, the device was further used as a robust, ultra-sensitive, and self-powered piezoelectric sensor for application in intelligent sports (Fig. 5). By attaching the device to an athlete's body, football and football ground, respectively, it can accurately monitor the football practice activities in real time. The comparative analysis of piezoelectric signals from different sources definitely ensures accurate, comprehensive information is acquired from surrounding environment and human activities. The transient device possesses the ability to collect and analyze athletic big data, thus having the potential for application in digital-twin-based smart sports systems [4,29].

## 4. Conclusion

In summary, we have developed a novel class of multifunctional, physically transient piezoelectrets using electrospun CIS-QDs/S–CNCs/PHB-based highly-oriented electret fibers. The striking merits included large Stokes shifted red-luminescence, composting environment degradation, and dynamic self-polarization-enhanced piezoresponse. The first use of $CuInS_2$-based QDs doping in natural biopolymers showed that small, yet moderate amounts of CIS-QDs allowed for preferential orientation growth of piezoelectric phase PHB lamellae. The significant piezoelectric enhancement was thus achieved by a synergistic action of the CIS-QDs-constrained, highly-oriented intrinsic micro-dipoles of PHB molecules and the artificial, dynamically-active macro-dipoles of S–CNCs. Under a 20-N, 4-Hz impulse force, the piezoelectric output of CIS-QDs/S–CNCs/PHB-based device was almost 2 and 5 times higher

than that of S–CNCs/PHB-based and PHB-based devices, respectively. In a real scenario of football practice, the transient device as a flexible self-powered piezo sensor demonstrated the ability to collect/analyze athletic big data in intelligent sports. We believe this study may be beneficial to developing a new generation of transient materials/devices for applications in digital twins and metaverse.

## CRediT authorship contribution statement

**Zhu Liu:** Writing – original draft, Validation, Methodology, Investigation. **Yu Lai:** Investigation. **Juan Li:** Investigation. **Zhipei Xia:** Investigation. **Liang Lu:** Investigation. **Chuanfeng Wang:** Investigation. **Biyao Huang:** Investigation. **Chu Pan:** Investigation. **Jiashun Wen:** Investigation. **Weiqing Yang:** Supervision, Resources. **Jun Lu:** Writing – review & editing, Supervision, Resources, Funding acquisition, Conceptualization.

## Declaration of competing interest

The authors declare that they have no known competing financial interests or personal relationships that could have appeared to influence the work reported in this paper.

## Data availability

Data will be made available on request.

## Acknowledgements

This work was financially supported by National Natural Science Foundation of China (No. 52073237).

## Appendix A. Supplementary data

Supplementary data to this article can be found online at https://doi.org/10.1016/j.coco.2024.101919.

## References

[1] T. Jin, Z. Sun, L. Li, Q. Zhang, M. Zhu, Z. Zhang, G. Yuan, T. Chen, Y. Tian, X. Hou, C. Lee, Triboelectric nanogenerator sensors for soft robotics aiming at digital twin applications, Nat. Commun. 11 (2020) 5381.
[2] G. Coorey, G.A. Figtree, D.F. Fletcher, J. Redfern, The health digital twin: advancing precision cardiovascular medicine, Nat. Rev. Cardiol. 18 (2021) 803–804.
[3] P. Bauer, B. Stevens, W. Hazeleger, A digital twin of Earth for the green transition, Nat. Clim. Change 11 (2021) 80–83.
[4] Z. Zhang, F. Wen, Z. Sun, X. Guo, T. He, C. Lee, Artificial intelligence-enabled sensing technologies in the 5G/internet of things era: from virtual reality/augmented reality to the digital twin, Adv. Intell. Syst. 4 (2022) 2100228.
[5] Y. Yang, Q. Shi, Z. Zhang, X. Shan, B. Salam, C. Lee, Robust triboelectric information-mat enhanced by multi-modality deep learning for smart home, InfoMat 5 (2023) e12360.
[6] S.-W. Hwang, H. Tao, D.-H. Kim, H. Cheng, J.-K. Song, E. Rill, M.A. Brenckle, B. Panilaitis, S.M. Won, Y.-S. Kim, Y.M. Song, K.J. Yu, A. Ameen, R. Li, Y. Su, M. Yang, D.L. Kaplan, M.R. Zakin, M.J. Slepian, Y. Huang, F.G. Omenetto, J. A. Rogers, A physically transient form of silicon electronics, Science 337 (2012) 1640–1644.
[7] W. Jiang, H. Li, Z. Liu, Z. Li, J. Tian, B. Shi, Y. Zou, H. Ouyang, C. Zhao, L. Zhao, R. Sun, H. Zheng, Y. Fan, Z.L. Wang, Z. Li, Fully bioabsorbable natural-materials-based triboelectric nanogenerators, Adv. Mater. 30 (2018) 1801895.
[8] M. Jian, Y. Zhang, Z. Liu, Natural biopolymers for flexible sensing and energy devices, Chin. J. Polym. Sci. 38 (2020) 459–490.
[9] F. Yang, J. Li, Y. Long, Z. Zhang, L. Wang, J. Sui, Y. Dong, Y. Wang, R. Taylor, D. Ni, W. Cai, P. Wang, T. Hacker, X. Wang, Wafer-scale heterostructured piezoelectric bio-organic thin films, Science 373 (2021) 337–342.
[10] Y. Zhu, C. Romain, C.K. Williams, Sustainable polymers from renewable resources, Nature 540 (2016) 354–362.
[11] C. Wang, T. Yokota, T. Someya, Natural biopolymer-based biocompatible conductors for stretchable bioelectronics, Chem. Rev. 121 (2021) 2109–2146.
[12] M. Gao, Y. Wang, S. Li, J. Liu, A. Feng, G. Zhang, L. Zhang, Design and fabrication of recyclable and reshape vitrified elastomer reinforced with renewable cellulose nanocrystal, Compos. Commun. 32 (2022) 101165.
[13] S. Yasin, M. Hussain, Q. Zheng, Y. Song, Influence of ionic liquid on rheological behaviors of candle soot and cellulose nanocrystal filled natural rubber nanocomposites, Compos. Commun. 33 (2022) 101214.
[14] Z. Ma, T. Xue, Q. Wali, Y.-E. Miao, W. Fan, T. Liu, Direct ink writing of polyimide/bacterial cellulose composite aerogel for thermal insulation, Compos. Commun. 39 (2023) 101528.
[15] C. Wang, Z. Peng, X. Huang, C. Yan, T. Yang, C. Zhang, J. Lu, W. Yang, Expecting the unexpected: high pressure crystallization significantly boosts up triboelectric outputs of microbial polyesters, J. Mater. Chem. A 9 (2021) 6306–6315.
[16] C. Wang, L. Lu, W. Li, D. Shao, C. Zhang, J. Lu, W. Yang, Green-in-green biohybrids as transient biotriboelectric nanogenerators, iScience 25 (2022) 105494.
[17] L. Lu, C. Wang, Z. Liu, Y. Lai, W. Li, D. Shao, J. Lu, W. Yang, Natural bioproducts' hybridization creates transient dynamic electret nanogenerators, J. Mater. Chem. C 11 (2023) 11034–11045.
[18] M.R. Bergren, N.S. Makarov, K. Ramasamy, A. Jackson, R. Guglielmetti, H. McDaniel, High-performance $CuInS_2$ quantum dot laminated glass luminescent solar concentrators for windows, ACS Energy Lett. 3 (2018) 520–525.
[19] Z. Long, W. Zhang, J. Tian, G. Chen, Y. Liu, R. Liu, Recent research on the luminous mechanism, synthetic strategies, and applications of $CuInS_2$ quantum dots, Inorg. Chem. Front. 8 (2021) 880–897.
[20] B. Chen, W. Zheng, F. Chun, X. Xu, Q. Zhao, F. Wang, Synthesis and hybridization of $CuInS_2$ nanocrystals for emerging applications, Chem. Soc. Rev. 52 (2023) 8374–8409.
[21] C. Xu, L. Zhang, Y. Xu, Z. Yin, Q. Chen, S. Ma, H. Zhang, R. Huang, C. Zhang, L. Jin, W. Yang, J. Lu, Filling the holes in piezopolymers with a solid electrolyte: a new paradigm of poling-free dynamic electrets for energy harvesting, J. Mater. Chem. A 5 (2017) 189–200.
[22] J. Xue, T. Wu, Y. Dai, Y. Xia, Electrospinning and electrospun nanofibers: methods, materials, and applications, Chem. Rev. 119 (2019) 5298–5415.
[23] Q. Qiu, M.M. Zhu, Z.L. Li, K.L. Qiu, X.Y. Liu, J.Y. Yu, B. Ding, L. Tang, J. Dai, Y.-T. Liu, Z.-L. Li, T.-F. Yi, L. Cai, J. Yu, B. Ding, Black phosphorus quantum dots supported by a conductive polymer nanofibrous membrane: a self-standing, metal-free electrocatalyst for nitrogen fixation, Compos. Commun. 23 (2021) 100551.
[24] A. Yin, J. Wang, S. Hu, M. Sun, B. Sun, M. Dong, T. Zhang, Z. Feng, H. Zhang, B. Shi, C. Zhang, H. Liu, High performance waterproof-breathable fully flexible tactile sensor based on piezotronics coupled OFET, Nano Energy 106 (2023) 108034.
[25] Y. Xu, L. Jin, X. He, X. Huang, M. Xie, C. Wang, C. Zhang, W. Yang, F. Meng, J. Lu, Glowing stereocomplex biopolymers are generating power: polylactide/carbon quantum dot hybrid nanofibers with high piezoresponse and multicolor luminescence, J. Mater. Chem. A 7 (2019) 1810–1823.
[26] G. Nolze, R. Hielscher, Orientations - perfectly colored, J. Appl. Crystallogr. 49 (2016) 1786–1802.
[27] C. Su, G. Shi, X. Li, X. Zhang, A.J. Müller, D. Wang, G. Liu, Uniaxial and mixed orientations of poly(ethylene oxide) in nanoporous alumina studied by X-ray pole figure analysis, Macromolecules 51 (2018) 9484–9493.
[28] R. Gerhard-Multhaupt, Less can be more - holes in polymers lead to a new paradigm of piezoelectric materials for electret transducers, IEEE Trans. Dielectr. Electr. Insul. 9 (2002) 850–859.
[29] J. Luo, W. Gao, Z.L. Wang, The triboelectric nanogenerator as an innovative technology toward intelligent sports, Adv. Mater. 33 (2021) 2004178.